Mass spectrometric multiple soil-gas flux measurement system with portable high-resolution mass spectrometer MULTUM coupled to automatic chamber for continuous field observation

Noriko Nakayama[1], Yo Toma[2], Yusuke Iwai[3], Hiroshi Furutani[1,4], Toshinobu Hondo[5], Ryusuke Hatano[6], and Michisato Toyoda[1]

[1]Graduate School of Science, Osaka University, Toyonaka, Osaka 560-0043, Japan
[2]Graduate School of Agriculture, Ehime University, Matsuyama, Ehime 790-8566, Japan
[3]Graduate School of Science, Osaka University, Toyonaka, Osaka 560-0043, Japan
[4]Center for Scientific Instrument Renovation and Manufacturing Support, Osaka University, Toyonaka, Osaka 560-0043, Japan
[5]Graduate School of Science, Osaka University, Toyonaka, Osaka 560-0043, Japan
[6]Research Faculty of Agriculture, Hokkaido University, Sapporo, Hokkaido 060-8589, Japan

Correspondence to: Noriko Nakayama (nnakayama@ess.sci.osaka-u.ac.jp)

Abstract. We developed a mass spectrometric soil-gas flux measurement system using a portable high-resolution multiturn time-of-flight mass spectrometer, called MULTUM, and we combined it with an automated soil-gas flux chamber for the continuous field measurement of multiple gas concentrations with a high temporal resolution. The developed system continuously measures the concentrations of four different atmospheric gases (N_2O, CH_4, CO_2, and O_2) ranging over six orders of magnitude at one time using a single gas sample. The measurements are performed every 2.5 min with an analytical precision (two standard deviations) of ±34 ppbv for N_2O; ±170 ppbv, CH_4; ±16 ppmv, CO_2; and ±0.60 vol%, O_2 at their atmospheric concentrations. The developed system was used for the continuous field soil–atmosphere flux measurements of greenhouse gases (N_2O, CH_4, and CO_2) and O_2 with a 1 h resolution. The minimum quantitative fluxes (two standard deviations) were estimated via a simulation as 70.2 μg N m^{-2} h^{-1} for N_2O; 139 μg C m^{-2} h^{-1}, CH_4; 11.7 mg C m^{-2} h^{-1}, CO_2; and 9.8 g O_2 m^{-2} h^{-1}, O_2. The estimated minimum detectable fluxes (two standard deviations) were 17.2 μg N m^{-2} h^{-1} for N_2O; 35.4 μg C m^{-2} $^{-1}$, CH_4; 2.6 mg C m^{-2} h^{-1}, CO_2; and 2.9 g O_2 m^{-2} h^{-1}, O_2. The developed system was deployed in the university farm of the Ehime University (Matsuyama, Ehime, Japan) for a field observation over five days. An abrupt increase in N_2O flux from 70 to 682 μg N m^{-2} h^{-1} was observed a few hours after the first rainfall, whereas no obvious increase was observed in CO_2 flux. No abrupt N_2O flux change was observed in succeeding rainfalls, and the observed temporal responses at the first rainfall were different from those observed in a laboratory experiment. The observed differences in temporal flux variation for each gas component show that gas production processes and their responses for each gas component in the soil are different. The results of this study indicate that continuous multiple-gas concentration and flux measurements can be employed as a powerful tool for tracking and understanding underlying biological and physicochemical processes in the soil by measuring more tracer gases such as volatile organic carbon, reactive nitrogen, and noble gases and by exploiting the broad versatility of mass spectrometry in detecting a broad range of gas species.

1 Introduction

Soil acts either as a source or a sink for various atmospheric gases such as greenhouse gases (GHGs: N_2O, CO_2, and CH_4) (Oertel *et al*., 2016; Ito *et al*., 2018), oxygen (O_2) (Turcu *et al*., 2005, Huang *et al*., 2018), and biogenic volatile organic compounds (BVOCs) (Insam and Seewald, 2010; Peñuelas *et al*., 2014; Szog *et al*., 2017, Mäki *et al*., 2019). Behaviors related to either emitting or absorbing soil gases and their magnitudes depend considerably on soil properties such as biological and physicochemical characteristics of the soil, which are in turn affected by environmental factors such as soil temperature, moisture, nutrients, pH level, rainfalls, and redox state (Dick *et al*. 2001; Rowlings *et al*., 2012; Luo *et al*., 2013, Li *et al*., 2015, Arias-Navarro *et al*., 2017; Pärn *et al*., 2018). Soil conditions and environmental factors vary within minutes to hours, and therefore, soil gases are expected to vary on a similar time scale. Thus, for accurate soil gas flux estimation, continuous measurement with a high temporal resolution is necessary to capture these rapid variations and employ them to estimate average fluxes.

Although the soil-atmosphere flux measurements of GHGs have been extensively performed because of their environmental effects, other soil gas measurements have been less frequently conducted despite these gases providing valuable biological and physicochemical insights about the soil. For example, O_2 concentration can be measured to quantify biological processes because the O_2 content in a soil is closely related to the respiration of soil organisms in the soil. Further, the redox state in soil has a significant effect on biological GHGs generation processes such as nitrification/denitrification (Hall *et al*., 2013, Heil *et al*., 2016) and methane production/oxidation (Kaiser *et al*., 2018); it is considerably useful to deduce the biological status of rice paddy soils (Lee *et al*., 2015). The BVOCs are produced by soil microorganisms, soil fungi, and even plant roots (Peñuelas *et al*., 2014), and they does not seem to be a simple intermediate/final product of the metabolic cycles and microbial decomposition of organic matter. Instead, they play unique roles such as signaling among microorganisms, fungi, and plant roots activities in soil (Peñuelas *et al*., 2014). Noble gases are biologically and chemically inert and can therefore be used as a tracer for physical processes if combined with biologically active soil gases. Using noble gases as tracers allow separating biological and physical components when determining the behavior of biologically active gases (Yang and Silver, 2012). The concentration of O_2/Ar has been used in aquatic systems to estimate net O_2 productions (Kana *et al*., 1994; Nakayama *et al*., 2002). Thus, the simultaneous measurement of multiple soil gases with a higher time resolution is expected to be considerably advantageous to gain a better understanding of soil biological and physicochemical processes and to gauge their environmental effects. However, such simultaneous measurements of multiple soil gases remain challenging because of the lack of suitable measurement technology.

To measure the concentrations of GHGs (CO_2, N_2O, CH_4, SF_6, and CO) and BVOCs in soil air, gas chromatography (GC) analysis has been extensively used; however, it requires different measurement configurations and settings for each gas species because all gases have different physicochemical properties and concentrations. For example, a GC coupled to an electron capture detector (GC-ECD) has been used for N_2O and SF_6, while a GC coupled to a flame ionization detector (GC-FID) has been used for carbon-containing gases such as CH_4, CO_2, and CO. However, there are only a few studies in which

multiple gases in soil are analyzed using a single GC system, *e.g.*, N_2O, CO_2, and CH_4 (Christiansen *et al*., 2015, Brannon *et al*., 2016); N_2O, CO_2, CH_4, and CO (van der Laan *et al*., 2009); and N_2O, CO_2, CH_4, CO, and SF_6 (Lopez *et al.*, 2015). Although these studies claimed that multiple soil gases were measured using by a single GC system, several sub-GC systems optimized for different target gases (*e.g.*, GC-ECD, GC-FID with different columns and settings) were integrated into a single GC system. This complexity hinders the simultaneous measurement of multiple soil gases by the GC system.

The recently advanced optical technique of cavity ring-down spectroscopy enables simultaneous measurement of multiple GHGs (N_2O, CO_2, and CH_4) from soils; it has been successfully applied for simultaneous gas flux measurements of multiple GHGs with a temporal resolution of minutes to tens of minutes (Christiansen *et al*., 2015, Brannon *et al*., 2016, Lebegue *et al*., 2016, Barba *et al*., 2019, Courtois *et al*., 2019). Despite the advantages of cavity ring-down spectroscopy, its application is limited to GHGs because infrared absorption wavelengths of gases often overlap and experience interference with other gases. This makes it necessary to perform appropriate water vapor corrections for accurate measurement, and thus, it is not yet applied for the measurement of trace gases (*e.g.*, NO, SF_6), noble gases, and complex BVOCs in soil air.

Mass spectrometry (MS) provides high sensitivity and allows detecting a wide range of chemicals as it is widely used for the trace analysis of various compounds including multiple BVOCs measurements with proton-transfer reaction mass spectrometry (PTR-MS) (Veres *et al*., 2014, Mancuso *et al*., 2015, references in Peñuelas *et al*., 2014, Yuan *et al*., 2017). However, the application of MS to the simultaneous measurement of various GHGs is limited by the difficulty in resolving CO_2 and N_2O. In fact, CO_2 and N_2O have considerably similar mass (43.989 and 44.001 u, respectively), and their ion peaks are difficult to distinguish using ordinary mass spectrometers such as quadrupole mass spectrometers that do not have sufficient high-mass resolving power to resolve ions. The independent detection of CO_2^+ and N_2O^+ by MS requires a mass-resolving power above 10,000, which corresponds to high-resolution spectrometry that can be achieved by mass spectrometers used in laboratories.

Recently, simultaneous mass spectrometric field measurement of multiple GHGs has become feasible (Anan *et al*., 2014), after the introduction of a portable high-resolution multiturn time-of-flight mass spectrometer (MULTUM; Shimma *et al*., 2010), which has dimensions comparable to that of a desktop PC (215 × 545 × 610 mm, 45 kg) and a high mass resolving power (30,000–50,000) for direct mass spectrometric separation of natural gas mixtures. Although MULTUM can resolve CO_2^+ and N_2O^+ ion peaks, it is technically difficult to measure the two GHGs and major atmospheric gas components (N_2 and O_2) simultaneously. This is because their concentrations in air substantially differ by more than six orders of magnitude (78.1%, 20.9%, 405 ppmv, and 330 ppbv for average atmospheric N_2, O_2, CO_2, and N_2O, respectively) and because MULTUM has a limited dynamic range of ion detection and signal acquisition. In addition, suppression in the electron ionization source causes major gases to restrict the ionization of other trace gases, which undermines sensitivity to the latter. Even using MULTUM, these inherent restrictions in MS need to be mitigated for the simultaneous measurement of atmospheric gases such as N_2O, CH_4, CO_2, and O_2, for which the concentrations span over six orders of magnitude. Thus far, the lack of field portable high-resolution MS and technical difficulties in existing ion detectors and signal acquisition and processing prevented the simultaneous field observation of multiple GHGs.

In this study, we combined MULTUM with a hybrid ion detectioFcampan and signal processing technique to measure multiple gases with different concentrations over six orders of magnitude in a single measurement quantitatively and simultaneously. We used the high-resolution MS system to measure the concentrations of N_2O, CH_4, CO_2, and O_2 every 2.5 min. The system was coupled with an automated open/closed chamber as the MULTUM–soil chamber system to obtain hourly soil–atmosphere gas fluxes. We detail the proposed system and its characterization, including the simultaneous gas flux observations under both laboratory settings and at an agricultural field.

2 Materials and methods

2.1 Simultaneous GHGs and O_2 measurement using MULTUM

Figure 1 illustrates the MULTUM–soil chamber system that comprises an automatic open/closed chamber, a sample/standard gas injection unit, and a mass spectrometer. The chamber was developed at Hokkaido University. The gas-tight lid of the custom chamber (0.25 × 0.37 m, inner diameter × height, 0.02 m^3 internal volume) is opened or closed by a DC motor attached to the chamber. The lid aperture timing is controlled using an FPGA platform (DE0-Nano-SoC Development Kit, Terasic, Hsinchu, Taiwan) with a Linux shell script through the "curl" command on a workstation. The system clocks of both the embedded Linux software and the workstation are synchronized using the IEEE 1588-2008 protocol, which obtains a sub-microsecond time difference.

The soil gas in the chamber headspace is continuously circulated through stainless-steel tubing (1/8 inch × 10 m, outer diameter × length) between the chamber and the sample injection unit via an air pump (CM-15-12, Enomoto Micro Pump, Tokyo, Japan). The circulating soil gas continuously passes through a 100 μL sample loop (SL100CM, Valco Instruments, Houston, TX, USA) fitted to a port with a six-port auto valve (V_1) (SAV-VA-11-65, FLOM, Tokyo, Japan). When the collected sample gas is analyzed with MULTUM (infiTOF-UHV, MSI Tokyo, Tokyo, Japan), the valve rotates and the soil gas sample is injected into a porous layer open tubular capillary column with a monolithic carbon layer (15 m × 0.320 mm, length × inner diameter, 3.0 μM; GS-Carbon PLOT, Agilent Technologies, Santa Clara, CA, USA) with a carrier He gas stream (2.5 mL/min) for rough gas separation before feeding into MULTUM. Another six-port auto valve (V_2) (SAV-VA-11-65, FLOM, Tokyo, Japan) switches soil-gas sampling and standard gas injection for calibration. Sample gas injection occurs every 2.5 min, and both the sample and standard gas injections are controlled by the FPGA.

Although MULTUM has sufficient mass resolving power for completely separating CO_2^+ and N_2O^+ ion peaks, we include the column to provide slight time lags between N_2/O_2, CO_2, and N_2O before injection into the system to improve quantification. In fact, omitting the separation in the time domain (20–60 s) causes several intrinsic MS problems. For example, the N_2O^+ is derived directly from co-existing N_2 and O_2 at the electron impact (EI) source reaction. Further, the ionization of atmospheric trace gases with the main components of the atmosphere (*e.g.*, N_2, O_2) restrict the ionization of co-existing trace gases in the ion source (ion-source saturation), which considerably worsens the detection limit of the trace gases. Finally, the dynamic ranges of the ion detector and signal acquisition are limited to two to three orders of magnitude, thereby impeding the

simultaneous and accurate measurement of N_2O and CO_2 within a single gas sample wherein the concentrations differ by more than three orders of magnitude. Thus, we adopt a hybrid ion detection and signal processing technique that selects either waveform averaging or ion counting to detect ions with intensities differing by six orders of magnitude (Kawai *et al*., 2018).

In the conventional waveform averaging mode, it is difficult to recognize considerably less abundant ions (*e.g.*, N_2O^+) as an ion peak because such low abundant ions are easily overwhelmed by background noise. In contrast, ion counting allows detecting scarce ions (Hoffmann and Stoobant, 2007) by regarding ion peaks above a pre-defined threshold intensity (−10 mV in this study) as a single ion. However, counting loss occurs for abundant ions when two or more ions arrive at the detector within the minimum time resolution of the ion signal detection system. The present hybrid ion detection and signal processing scheme employs two detection modes using a single ion detector and recording system by selecting either waveform averaging or ion counting depending on the type of gas (at different periods from sample injection into the column) by changing the ion detector gain and real-time signal processing protocol (Hondo *et al*., 2017). Thus, a column is required to create small temporal separations for the detection of target ions and to select the appropriate measurement mode in addition to averting ion-source saturation. For the detection of CO_2^+, the ion detector voltage is set to 2400 V, and the conventional waveform recording and averaging are conducted for the time-of-flight ion signal where the voltage is set to 2650 V for the detection of O^+, CH_4^+, and N_2O^+; the real-time software thresholding (*i.e.*, ion counting) is conducted for the acquired signal (Fig. 2). Oxygen was detected as O^+ (not as O_2^+) using the ion counting mode because O^+ (*m/z* 15.99) can be simultaneously detected along with CH_4^+ (*m/z* 16.03). If oxygen is observed as O_2^+ (*m/z* 32.00), another mass segment around *m/z* 32.00 needs to be analyzed, and less measurement time can be allocated for CH_4^+ and N_2O^+ measurements, which results in lower sensitivity for CH_4^+ and N_2O^+ measurements. The optimized high-voltage settings of MULTUM for this study are listed in Table 1.

The gases injected into MULTUM are ionized by electron ionization at an electron acceleration voltage of 30 V, and the produced ions are mass analyzed at a repetition rate of 1 kHz with 30 laps of circular ion flight; this yields a mass resolution of approximately 10,000. After 30 laps, each ion is detected by an electron multiplier (ETP secondary electron multiplier 14882, ETP Ion Detect, Sydney, Australia). The ion signal from the ion detector is then amplified through a high-speed preamplifier (ORTEC 9301, Advanced Measurement Technology, Oak Ridge, TN, USA) and recorded and processed in real time with a high-speed 1 GS/s digitizer (U5303a, Keysight Technologies, Santa Rosa, CA, USA). Mass spectra are then transferred to a host PC (dual Intel 8-core/16-thread Xeon processor PC with Linux Debian 9.9 operating system). The data acquisition system is controlled by the QtPlatz open-source-software (https://github.com/qtplatz) with its plugin developed for the infiTOF system (Hondo *et al*., 2017, Jensen *et al*., 2017).

We calibrate the system with six different concentrations including blank gas (ultrapure N_2), which are prepared from mixed standard gases (mixture of N_2O, CH_4, and CO_2) and O_2 standard gas by diluting with ultrapure N_2 (>99.9995%, Takachiho Chemical Industrial, Tokyo, Japan). We use two certified standard gases (standard #1: N_2O, 279 ppbv; CH_4, 1.47 ppmv; CO_2, 421 ppmv in N_2; standard #2: N_2O, 1752 ppbv; CH_4, 2.97 ppmv; CO_2, 1705 ppmv in N_2; Sumitomo Seika Chemicals, Osaka, Japan) and O_2 standard gas (20.9% in N_2 balance gas; Takachiho Chemical Industrial, Tokyo, Japan). The

gas mixing rates are adjusted using mass flow controllers (Model 8500 series, KOFLOC, Kojima Instruments, Kyoto, Japan) calibrated using a soap film flowmeter (HORIBA STEC, Kyoto, Japan).

We continuously measured the standard gases using the developed MULTUM–soil chamber system and estimated the detection limits for N_2O, CO_2, CH_4, and O_2 based on the IUPAC criteria (Long and Winefordner, 1983) given as

$$LOD = k \cdot RSD/m, \quad (1)$$

where k is a constant that determines the confidence level (we set $k = 3$ for a confidence level above 99%), RSD is the standard deviation of the ion count or peak area of the target gas when measuring ultrapure N_2, and m is the slope of linear regression obtained from the measurement of the six above mentioned gas concentrations prepared from the standard gases and ultrapure N_2 based on 10 replicate measurements of each gas.

2.2 Flux measurement using MULTUM–soil chamber system

The fluxes of target soil gases are determined from the variation in the target gas concentration while the chamber is closed. During each flux measurement, nine consecutive measurements are conducted over 20 min. A complete flux measurement is performed once per hour. The chamber is closed during the first 20 min of the flux measurement, and it remains open during the remaining 40 min. The standard #2 and atmospheric air measurements are conducted to monitor the MULTUM stability (Fig. 3). The standard gas measurement is repeated five times and atmospheric air measurement is repeated ten times when the chamber is open. The fluxes of observed soil gases are calculated as (Minamikawa *et al.*, 2015)

$$Flux = \frac{\Delta C}{\Delta t} \cdot \frac{V}{A} \cdot \rho \cdot \frac{273}{273+T} \cdot \alpha, \quad (2)$$

where $\Delta C/\Delta t$ is the concentration variation of the target gas during the flux measurement period, V is the chamber volume (m^3), A is the chamber area (m^2), ρ is the gas density (kg m^{-3}), T is mean air temperature inside the chamber (°C), and α is a conversion factor to transform N_2O into N, and CH_4, CO_2 into C. We determine $\Delta C/\Delta t$ by applying linear regression to the data obtained from the nine consecutive concentration measurements when the chamber is closed.

Besides the flux measurement, we monitor soil temperatures and moisture with a portable digital thermometer (EM50 Data Logger, METER Group, Pullman, WA, USA). Further, we monitor the air temperature inside the chamber and the ambient temperature using a temperature data logger (Thermo Recorder TR-52i, T&D Corporation, Nagano, Japan).

The minimum detectable flux (MDF) of each soil gas can be estimated based on the derivations by Courtois *et al*. (2019) originally developed by Christiansen *et al*. (2015) and Nickerson (2016) as

$$MDF_i = \left(\frac{1}{t_c} \cdot \frac{A_{a,i}}{\sqrt{n}}\right)\left(\frac{V \cdot P}{S \cdot R \cdot T}\right), \quad (3)$$

where $A_{a,i}$ is the analytical accuracy of MULTUM for gas i, t_c is the closure time of the soil flux chamber per flux measurement (20 min), n is the number of gas concentration measurements to calculate the gas flux (*i.e.*, nine measurements), V is the volume of the flux chamber (0.018 m^3), P is the atmospheric pressure in kPa, S is the inner surface area of the flux

chamber (0.049 m^2), R is the ideal gas constant (8.314 m^3 Pa K^{-1} mol^{-1}), and T is the ambient temperature surrounding the chamber in K.

The MDF metric is a common performance metric in flux measurements; in particular, it is used in flux measurement methods based on continuous gas concentration observation with the chamber technique. Because MDF is a useful metric for comparing results between CRDS and our MS-based instrument, we employed the MDF for the comparison. The device accuracy ($A_{a,\,i}$) is defined as the measurement accuracy of an instrument (Christiansen *et al.* 2015; Nickerson 2016). In the flux measurement with the CRDS instrument, we use the accuracy value provided by the manufacturer. For our system, we define the analytical accuracy ($A_{a,i}$) as the analytical precision (measurement uncertainty) of MULTUM for gas i and use two standard deviations (2σ) obtained from 994 measurements of the gas in air. Here, the minimum detectable flux (MDF) is not a practical measure for the reliable quantification of flux. We additionally evaluate the minimum quantitative flux (MQF) for each gas as a quantitatively reliable flux in our study. Since flux is the rate of increase or decrease in the gas concentration of interest in the closed chamber, we determine the flux by applying linear regression to every set of the nine consecutive gas concentration measurements in the closed chamber period over 20 min. The MQF is determined from the precision of the slopes (rates of gas concentration changes) in the flux measurement relative to the *true* slope. However, the *true* slopes are difficult to determine in actual field measurements, and therefore, we conducted a simulation study to characterize the MQF of the current instrument for each gas species.

We first defined *a true* flux value of the gas for the model simulation assuming that the flux remained constant when the chamber is closed. Based on the defined true flux value and chamber dimension, *true* gas concentrations to be measured in the chamber were calculated over time when the chamber was closed. To simulate a realistic observation, a random measurement error based on the standard deviation derived from the atmospheric gas measurements was intentionally added to the predefined *true* gas concentrations when the chamber was closed. The simulated nine consecutive observation data were then used for flux determination with linear regression analysis, whose results were further characterized for MQF estimation. For each defined flux value, 10,000 sets of flux measurements were simulated, 10,000 corresponding slopes were obtained, and the standard deviations of the slopes were characterized. The simulation was conducted on a scientific graphical data processing software (Igor Pro, WaveMetrics, Lake Oswego, OR, USA) and the random measurement error was generated with a built-in Gaussian distribution noise generator.

2.3 Laboratory tests

We conducted laboratory flux measurement tests of N_2O, CH_4, CO_2, and O_2 using a soil sample collected at the university farm of Ehime University. The soil was collected from 0–10 cm below the soil surface. After sampling, the soil was sieved to remove roots and stones. A urea solution ($CO(NH_2)_2$) was added to the soil (4 g of urea to 1 kg of soil) to promote N_2O production. Then, the soil was air dried for a few days prior to flux measurement. The soil was spread in a 60 L plastic container, and the automated flux chamber was placed on the soil. The flux measurement cycle was the same as that used for the field observation shown in Fig. 3 (chamber is closed for 20 min; flux measurement with nine concentration measurements every

2.5 min; and chamber is open for the remaining 40 min). When the chamber was open, the standard gas and atmospheric air measurements were conducted for system calibration and verification. After 22 h from the start of the laboratory flux measurement, 3 L of water was sprayed on the soil for initiating the production or consumption of CO_2, CH_4, and N_2O, and the flux measurement proceeded for 46 h.

2.4 Field observations

We deployed the developed MULTUM–soil chamber system at the university farm of Ehime University (Matsuyama-shi, Ehime, Japan) for a field observation over five days (September 3–8, 2018). The university farm is used for various agricultural production and soil studies (Toma, *et al.*, 2019, Asagi and Ueno, 2009).

The automated flux chamber was placed on a ridge in the upland field, as shown in the left panel of Fig. 4. The field test was conducted during the fallow period (*i.e.*, bare field condition). The soil pH, electric conductivity, and texture were 5.3, 34.0 μS cm^{-1}, and sandy loam (sand, 75.6%; silt, 10.6%; clay, 13.8%), respectively. On September 2, ammonium sulfate (150 kg N ha^{-1}) and dried cattle feces (10 Mg ha^{-1} of fresh weight) were added and incorporated into the soil surface (0–15 cm depth). After plowing, the soil bulk density and porosity were 1.02 g cm^{-3} and 62.9%, respectively. The automated soil chamber was installed immediately after incorporation. The total carbon (C) and nitrogen (N) contents of the dried cattle feces were 36.1 and 2.08%, respectively. The other components of the MULTUM–soil chamber system (*i.e.*, MULTUM platform, control, and data acquisition system) were installed at a nearby goat hut that had a room temperature of 27 ± 2°C. Two 5-m-long stainless-steel tubes (1/8 inch outer diameter) were used to connect the chamber and the six-port auto valve in the gas injection unit to circulate headspace gas within the chamber.

3 Results and discussion

3.1 Laboratory characterization of MULTUM–soil chamber system performance

In the laboratory, we characterized the performance of the developed MULTUM–soil chamber system by introducing standard gases through the gas injection unit at six different concentrations and by following the procedure for field observations. As shown in Fig. 5, MULTUM linearly responds to the gas concentrations during measurement, thereby obtaining coefficients of determination (R^2) for all linear regression results above 0.996. Blank concentrations checked by introducing ultrapure N_2 were very small compared to the atmospheric concentrations of the target gases. The calculated detection limits were 12 ppbv for N_2O; 50 ppbv, CH_4; 13 ppmv, CO_2; and 0.68 vol%, O_2, based on Eq. (2).

To verify the stability of the developed MULTUM–soil chamber system, we conducted continuous measurements of atmospheric N_2O, CH_4, CO_2, and O_2 in the laboratory with the flux chamber open (Fig. 6). The set of N_2O, CH_4, CO_2, and O_2 measurements was repeated every 2.5 min over 42 h. In the laboratory, the room temperature was maintained at 23 ± 1 °C and the relative humidity was around 15% at the beginning of the measurement; it increased to 30–33% after the midnight of January 31, 2019. The atmospheric pressure during the laboratory measurement period ranged between 1005–1014 hPa. The

variations of atmospheric N_2O, CH_4, CO_2, and O_2 measurements are shown as histograms in Fig. 7. Because the distributions agree with Gaussian distributions plotted as dashed lines in Fig. 7, we calculated the standard deviations (2σ) of each gas from the measurements to obtain frequency $A_{a,i}$. The $A_{a,i}$ obtained from the atmospheric air measurements were ±22 ppbv for N_2O; ±102 ppbv, CH_4; ±8.1 ppmv, CO_2; and ±0.38 vol%, O_2. These variations may be subject to the natural variabilities of atmospheric concentrations; however, we consider that they are instrumental variations because their distributions demonstrated good agreements with Gaussian distributions (Fig. 7) and the analytical precision obtained from the measurements of standard#1 and O_2 standard in the laboratory (±34 ppbv for N_2O; ±170 ppbv, CH_4; ±16 ppmv, CO_2; and ±0.60 vol%, O_2, 2σ) almost corresponded to those obtained from atmospheric air. Using the standard gas rather than ambient air usually yields better instrumental performance because ambient air contains considerably more complicated gas species including water vapor, which can affect the precision of mass spectrometric measurement. Our final goal in our instrumental development is to construct a new instrument for field observation; soil gas flux is determined from the change in gas concentration in the flux chamber relative to its atmospheric concentration. Thus, we considered that using ambient air measurement for out instrumental performance test is more appropriate and practical for our research purpose.

3.2 Laboratory flux measurement test

Before the field campaign, we conducted a laboratory flux measurement test to confirm whether our newly developed instrument could capture each soil gas flux when water was added, which is a major fluctuation factor of soil gas flux. The temporal variations of the measured gas concentrations when the chamber is closed is shown in Fig. 8. Only data acquired when the chamber is closed (flux measurement periods) is depicted for simplification; however, the system stability verification and calibration were conducted when the chamber is open. At 22 h, water (approximately 3 L) was sprayed on the soil surface as environmental perturbation resembling rainfall to reactivate the dormant soil biological processes. Immediately after water addition, the emission of N_2O and CO_2 began to change in different ways. For example, the CO_2 emission rapidly increased and reached its maximum 2 h after water addition and remained relatively high, whereas N_2O emission gradually increased until 20 h after water addition at a seemingly constant rate.

Such increases in soil CO_2 flux by rainfall or rewetting soil have been reported previously (Lee *et al.*, 2002; Smith and Owens, 2010; Gelfand *et al.*, 2015; Kostyanovsky *et al.*, 2019); it enhances microbial activity and population and boosts the availability of carbon and nutrients because of either rewetting or the assemblages (Fierer and Schimel, 2003; Iovieno and Bååth, 2008; Blazewicz *et al.*, 2014). A similar increase in N_2O flux on rewetting soil have been reported (Nobre *et al.*, 2001; Dobbie and Smith, 2003; Smith and Owens, 2010; Gelfand *et al.*, 2015; Schwenke and Haigh, 2016; Leitner *et al.*, 2017; Barba *et al.*, 2019; Kostyanovsky *et al.*, 2019), although very few research reported the simultaneous response of N_2O and CO_2 fluxes upon artificial watering (Smith and Owens, 2010; Gelfand *et al.*, 2015; Kostyanovsky *et al.*, 2019). Only Kostyanovsky *et al.* (2019) reported short-term flux changes of both CO_2 and N_2O upon simulated rainfall with a time resolution of 2 h. They showed that the simulated rainfall immediately triggered increases in both CO_2 and N_2O fluxes; however, the increase in CO_2 flux continued till about 3 h after the simulated rainfall, while that in N_2O flux continued till about 5 h after the simulated

rainfall. In the present laboratory test, CO_2 and N_2O fluxes showed different temporal behaviors from those observed by Kostyanovsky *et al.* (2019), although the observed N_2O flux change was similar to that observed by Leitner *et al*. (2017). We speculate that the slow increase in N_2O flux may reflect a slow building-up of nitrification and denitrification microorganisms after watering, although further studies that consider both the biological and physicochemical aspects of the soil gas formations are necessary for gain better understanding. The fluxes of CH_4 and O_2 during the laboratory test were below their minimum detectable fluxes.

3.3 Minimum detectable and minimum quantitative fluxes of GHGs and O_2

In Fig. 7, the frequencies of atmospheric concentrations of N_2O, CH_4, CO_2, and O_2 observed with the MULTUM–soil chamber system during the laboratory stability check (Fig. 6) are compiled as histograms. Their frequency distributions agree well with Gaussian distributions (plotted as dashed lines in Fig. 7), and thus, their standard deviations are considered to have the $A_{a,i}$ of the MULTUM–soil chamber system for each gas. The $A_{a,i}$ is defined as the analytical precision (measurement uncertainty) of MULTUM for gas *i* and the use of two standard deviations (2σ) obtained from 994 measurements of atmospheric gas as a reference.

We estimated the MDFs based on Eq. (3) using the $A_{a,i}$ for each gas, and we obtained 17.2 μg N m^{-2} h^{-1}, 35.4 μg C m^{-2} h^{-1}, 2.6 mg C m^{-2} h^{-1}, and 2.9 g O_2 m^{-2} h^{-1} for N_2O, CH_4, CO_2, and O_2, respectively. However, the MDF is not a practical measure for the reliable quantification of flux. Thus, we evaluated the MQF for each gas as the quantitatively reliable flux in our study via model simulation.

Figures 9(a)–(d) show the relationship between the *true* flux and the calculated fluxes from the simulation. The error bars in the figures represent error ranges of fluxes (2σ) determined from the simulation. The average fluxes determined by the simulation were almost equal to their corresponding true fluxes, and the errors were relatively constant. Here, we define MQF as the flux when the true flux is equal to the error (2σ) of the corresponding simulated flux. We obtained the MQFs of 70.2 μg N m^{-2} h^{-1} for N_2O; 139 μg C m^{-2} h^{-1}, CH_4; 11.7 mg C m^{-2} h^{-1}, CO_2; and 9.8 g O_2 m^{-2} h^{-1}, O_2. We consider the observed fluxes below the MQFs as qualitatively uncertain, and we do not use them in subsequent data analyses for this study.

We conducted data quality checks for the filed observation flux data using coefficients of determination (R^2) in the linear regression analysis for nine consecutive concentration measurements when the chamber was closed. Fig. 10 shows the relationships between observed fluxes and the corresponding R^2 in the N_2O and CO_2 flux derivation during field flux observation at Ehime University. The R^2 was approximately 0.4 at its MQF (70.2 μg N m^{-2} h^{-1}) in the N_2O flux observation. The data with R_2 = 0.4 in its linear regression analysis is regarded to have a statistically significant correlation, which supports that MQF is a reasonable metric for reliable quantification. In the field N_2O flux measurement, R^2 increased with an increase in the observed flux, which indicates that the improvement of quality in N_2O measurement (*i.e.*, detection limit and sensitivity) is desirable for more reliable determination, and in particular, under a low N_2O flux condition. All CO_2 flux measurements showed $R^2 > 0.9$, indicating that the present system is reliable for CO_2 flux determination. The observed fluxes of CH_4 and O_2 during the laboratory/field study were usually below their MDFs; however, during a different field campaign in March 2019

at the same field, the CH_4 flux above the MDF was observed (Fig. 12). For O_2 flux, the analytical precision for the current O_2 concentration measurement was ± 0.60 vol% (± 6000 ppmv). The current flux observation was under a dark condition and the CO_2 concentration change was caused by respiration of the soil organisms. Therefore, the increase in CO_2 concentration in the flux chamber is roughly equal to the decrease in O_2 concentration during flux measurement. As shown in Fig. 8, to capture the O_2 flux, an analytical precision of more than three orders of magnitude is necessary because the CO_2 concentration change is about 100 ppmv after water spraying. It is considerably difficult to achieve an improvement in measurement precision by more than three orders of magnitude. Although quantitative O_2 flux measurement is difficult, our developed instrument can detect the variation in O_2 concentration as a tracer for the redox state in soil environments (Kaiser *et al.*, 2018).

3.4 Field observation

The N_2O fluxes were mostly below 300 μg N m^{-2} h^{-1} and generally dependent on soil moisture, which substantially affected the production, consumption, and atmospheric exchange of GHGs (Davidson and Swank, 1986, Dobbie and Smith, 2003, Liebig *et al*. 2005, Ellert and Janzen 2008, Sainju *et al.*, 2012). An interesting event was observed in the N_2O flux on September 4. The N_2O flux abruptly increased from 70 to 682 μg N m^{-2} h^{-1} within a few hours after rainfall, while a sudden drop in CO_2 flux was observed. These observed responses exhibit sharp contrast with our laboratory flux measurement test, in which CO_2 flux showed a rapid increase while N_2O flux showed a slow sustained increase upon water spraying (Fig. 8). Various studies have reported an increase in the N_2O flux after rainfall (Nobre *et al*., 2001; Dobbie and Smith, 2003; Smith and Owens, 2010; Gelfand *et al*., 2015; Schwenke and Haigh, 2016; Leitner *et al*., 2017; Barba *et al*., 2019; Kostyanovsky *et al*., 2019) and similar increases in CO_2 flux after rainfall have also been reported (Lee *et al*., 2002; Smith and Owens, 2010; Gelfand *et al*., 2015; Kostyanovsky *et al*., 2019). However, no short-term responses of CO_2 and N_2O fluxes similar to our observation upon rainfall have been reported. Further, two heavier rainfalls occurred on September 5 and 7; however, the N_2O flux showed no obvious increase similar to that after the first rainfall. The different responses in N_2O flux may reflect the complexity in microbial and nutrient dynamics initiated in the soil upon rainfall (Gordon *et al*., 2008; Blazewicz *et al*., 2014), although further detailed studies that investigate both biological and physicochemical aspects of the soil gas formations are necessary to determine the causes of the response. The CO_2 flux, in contrast, remained constant except during rainfall periods, in which an abrupt decrease and quick recovery within several hours of the flux occurred. This can be attributed to the suppression of CO_2 permeation within the soil column caused by a capping effect of wet soil and different vertical distributions within the soil column; although these explanations are feasible, they require further temporal and spatial investigation.

4 Conclusion and Future perspectives

We developed a field-deployable MS-based multiple gas flux measurement system utilizing a portable high-resolution mass spectrometer (MULTUM) combined with an automated soil-gas chamber. The MULTUM was coupled with a short gas separation column to roughly separate atmospheric major and trace gases over a short period, and a new hybrid ion detection

and signal processing technique was employed to ensure a much wider dynamic range for quantitative and simultaneous measurement of multiple gas concentrations that differ by six orders of magnitude. The present hourly continuous gas flux measurement of multiple gas species clearly indicates its considerable advantage of capturing rapid and different temporal responses of different gas species toward sporadic abrupt environmental changes (*e.g.*, sudden rainfall), which provides more detailed understanding of underlying soil biological and physicochemical processes.

Further improvement in the detection limit and analytical precision is required for the accurate measurements of low GHG fluxes, in particular, for N_2O and CH_4. We believe that the improvement in the sensitivity by one order of magnitude can be achieved relatively easily by retrofitting a larger vacuum pump to the MULTUM (from 50 l/s to 250 l/s), using a higher mass measurement rate (from current 1 kHz to 10 kHz), and using a flux chamber with a lower ratio of the height to bottom area. The privilege of MS-based gas measurement in highly sensitive and wider range of detectable gas species, including reactive-nitrogen gases (*e.g.*, NO, NO_2), noble gases (*e.g.*, Ar, Ne), inorganic gases (*e.g.*, N_2, H_2, CO, H_2S), small organic gases (*e.g.*, ethylene) should be quite advantageous in providing deeper insights into soil microbiological ecosystems, physicochemical processes, and their responses to environmental perturbations. A wide variety of gas species such as He, Ar, and polychlorinated biphenyls have already applied by MULTUM (Jense *et al*.,2017, Kawai *et al.*, 2018, Shimma *et al*., 2013). Coupling proton transfer reaction (PTR) ionization source with the MULTUM can help detect a wider range of individual BVOCs and subsequently their soil-atmosphere fluxes, and our group is coupling a PTR ion source to MULTUM.

We expect that further instrumental improvements and further expansion in detectable gas species will boost providing deeper insights on the biological and physicochemical processes in soil and lead to more comprehensive their understanding.

Data Availability. Data are available upon request.

Author contributions. NN led this research project and conducted a major part of the study. YT coordinated the field campaign, assisted with the field flux measurement, and provided valuable feedback and advice for the field measurements. YI assisted in conducting a field test. TH constructed the hybrid ion detection and signal processing technique as well as the data analysis tools. HF developed a prototype of the multiple-gas measurement, MULTUM, system. RH and MT created the conceptual framework of this study. All authors discussed the results and contributed to the preparation of the final manuscript.

Competing interests. The authors declare that they have no conflict of interest.

Acknowledgments. We thank the supporting staff at the university Fam in Ehime University for their assistance during the field observation. Further, we thank Hisanori Matsuoka for his assistance in developing and optimizing the electrical systems, and

Toshio Ichihara for the fabrication of the soil chamber. This work was supported by JSPS Challenging Research (Exploratory) under grant number 17K20044.

Review statement. This paper was edited by Christian Brümmer and reviewed by two anonymous referees.

References

Anan, T., Shimma, S., Toma, Y., Hashidoko, Y., Hatano, R., and Toyoda, M.: Real time monitoring of gases emitted from soils using a multiturn time-of-flight mass spectrometer "MULTUM-S II", Environ. Sci: Proc. Imp., 16, 2752–2757, https://doi.org/10.1039/C4EM00339J, 2014.

Arias-Navarro, C., Díaz-Pinés, E., Klatt, S., Brandt, P., Rufino, M. C., Butterbach-Bahl, K., and Verchot, L. V.: Spatial variability of soil N_2O and CO_2 fluxes in different topographic positions in a tropical mountain forest in Kenya, J. Geophys. Res. Biogeosci., 122, 514–527, https://doi.org/10.1002/2016JG003667, 2017.

Asagi, N. and Ueno, H.: Nitrogen dynamics in paddy soil applied with various ^{15}N-labelled green manures, Plant Soil, 322, 251–262, https://doi.org/10.1007/s11104-009-9913-4, 2009.

Barba, J., Poyatos, R., and Vargas, R.: Automated measurements of greenhouse gases fluxes from tree stems and soils: magnitudes, patterns and drivers, Sci. Rep., 9, 1–13, https://doi.org/10.1038/s41598-019-39663-8, 2019.

Blazewicz, S. J., Schwartz, E., and Firestone, M. K.: Growth and death of bacteria and fungi underlie rainfall-induced carbon dioxide pulses from seasonally dried soil, Ecology, 95, 1162-1172, https://doi.org/10.1890/13-1031.1, 2014.

Brannon, E. Q., Moseman-Valtierra, S. M., Rella, C. W., Martin, R. M., Chen, X., and Tang, J.: Evaluation of laser-based spectrometers for greenhouse gas flux measurements in coastal marshes, Limnol. Oceanogr. Meth., 14, 466–476, https://doi.org/10.1002/lom3.10105, 2016.

Christiansen, J. R., Outhwaite, J., and Smukler, S. M.: Comparison of CO_2, CH_4 and N_2O soil-atmosphere exchange measured in static chambers with cavity ring-down spectroscopy and gas chromatography. Agric. For. Meteorol., 211–212, 48–57, https://doi.org/10.1016/j.agrformet.2015.06.004, 2015.

Courtois, E. A., Stahl, C., Burban, B., Van den Berge, J., Berveiller, D., Bréchet, L., Soong, J. L., Arriga, N., Peñuelas, J., and Janssens, I. A.: Automatic high-frequency measurements of full soil greenhouse gas fluxes in a tropical forest, Biogeosciences, 16, 785–796, https://doi.org/10.5194/bg-16-785-2019, 2019.

Davidson, E. A. and Swank, W. T.: Environmental parameters regulating gaseous nitrogen losses from two forested ecosystems via nitrification and denitrification, Appl. Environ. Microbiol., 52, 1287–1292, PMID: 16347234, PMCID: PMC239223, 1986.

Dick, L, Skiba, U., and Wilson, L.: The effect of rainfall on NO and N_2O emissions from Ugandan agroforest soils. Phyton-Annales Rei Botanicae, 41, 73–80, http://nora.nerc.ac.uk/id/eprint/1023, 2001.

Dobbie, K. E. and Smith, K. A.: Nitrous oxide emission factors for agricultural soils in Great Britain: the impact of soil water-filled pore space and other controlling variables, Glob. Change Biol., 9, 204-218, https://doi.org/10.1046/j.1365-2486.2003.00563.x, 2003.

Ellert, B. H. and Janzen, H. H.: Nitrous oxide, carbon dioxide and methane emissions from irrigated cropping systems as influenced by legumes, manure and fertilizer. Can. J. Soil Sci., 88, 207–217, https://doi.org/10.4141/CJSS06036, 2008.

Fierer, N. and Schimel, J. P.: A proposed mechanism for the pulse in carbon dioxide production commonly observed following the rapid rewetting of a dry soil, Soil Sci. Soc. Am. J., 67, 798–805, https://doi.org/10.2136/sssaj2003.0798, 2013.

Gelfand, I., Cui, M., Tang, J., and Robertson, G.P.: Short-term drought response of N_2O and CO_2 emissions from mesic agricultural soils in the US Midwest, Agric. Ecosyst. Environ. 212, 127–133, https://doi.org/10.1016/j.agee.2015.07.005, 2015.

Gordon, H., Haygarth, P. M., and Bardgett, R. D.: Drying and rewetting effects on soil microbial community composition and nutrient leaching, Soil Biol. Biochem., 40, 302–311, https://doi.org/10.1007/s00248-010-9723-5, 2008.

Hall, S. J., McDowell, W. H., and Silver, W. L.: When Wet Gets Wetter: Decoupling of moisture, redox biogeochemistry, and greenhouse gas fluxes in a humid tropical forest soil, Ecosystems, 16, 576–589, https://doi.org/10.1007/s10021-012-9631-2, 2013.

Heil, J., Vereecken, H., and Brüggemann, N.: A review of chemical reactions of nitrification intermediates and their role in nitrogen cycling and nitrogen trace gas formation in soil. Eur. J. Soil Sci., 67, 23–39, https://doi.org/10.1111/ejss.12306, 2016.

Hoffmann, E. and Stroobant, V.: Mass Spectrometry Principles and Applications, 3rd edition, Wiley, Chichester, England, 2007.

Hondo, T., Jensen, K. R., Aoki, J., and Toyoda, M.: A new approach for accurate mass assignment on a multi-turn time-of-flight mass spectrometer, Eur. J. Mass Spectrom., 23, 385–392, https://doi.org/10.1177/1469066717723755, 2017.

Huang, J., Huang, J., Liu, X., Li, C., Ding, L., and Yu, H.: The global oxygen budget and its future projection, Sci. Bull., 63, 1180–1186, https://doi.org/10.1016/j.scib.2018.07.023, 2018.

Insam, H., and Seewald, M. S.: Volatile organic compounds (VOCs) in soils, Biol. Fert. Soils, 46, 199–213, https://doi.org/10.1007/s00374-010-0442-3, 2010.

Iovieno, P. and Bååth, E.: Effect of drying and rewetting on bacterial growth rates in soil, FEMS Microbiol. Ecol., 65, 400–7, https://doi.org/10.1111/j.1574-6941.2008.00524.x, 2008.

Ito, A., Nishina, K., Ishijima, K., Hashimoto, S., and Inatomi, M.: Emissions of nitrous oxide (N_2O) from soil surfaces and their historical changes in East Asia: a model-based assessment, Prog. Earth Planet. Sci., 5, 55, https://doi.org/10.1186/s40645-018-0215-4, 2018.

Jensen, K. R., Hondo, T., Sumino, H., and Toyoda, M.: Instrumentation and method development for on-site analysis of helium isotopes, Anal. Chem., 89, 7535–7540, https://doi.org/10.1021/acs.analchem.7b01299, 2017.

Kana, T., Darkangelo, C., Hunt, M., Oldham, J., Bennett, G., and Cornwell, J.: Membrane inlet mass spectrometer for rapid high-precision determination of N_2, O_2, and Ar in environmental water samples, Anal. Chem., 66, 4166–4170, https://doi.org/10.1021/ac00095a009, 1994.

Kawai, Y., Hondo, T., Jensen, K. R., Toyoda, M., and Terada, K: Improved quantitative dynamic range of time-of-flight mass spectrometry by simultaneously waveform-averaging and ion-counting data acquisition, J. Am. Soc. Mass Spectrom., 29, 1403–1407, https://doi.org/10.1007/s13361-018-1967-1, 2018.

Kaiser, K. E., McGlynn, B. L., and Dore, J. E.: Landscape analysis of soil methane flux across complex terrain, Biogeosciences, 15, 3143-3167, https://doi.org/10.5194/bg-15-3143-2018, 2018.

Kostyanovsky, K. I., Huggins, D. R., Stockle, C. O., Morrow, J. G., and Madsen, I. J.: Emissions of N_2O and CO_2 following short-term water and N fertilization events in wheat-based cropping systems, Front. Ecol. Evol., 7, 63, https://doi.org/10.3389/fevo.2019.00063, 2019.

Laan, S. V. D, Neubert, R. E. M., and Meijer, H. A. J.: A single gas chromatograph for accurate atmospheric mixing ratio measurements of CO_2, CH_4, N_2O, SF_6 and CO, Atmos. Meas. Tech., 2, 549–559, https://doi.org/10.5194/amt-2-549-2009.

Lebegue, B., Schmidt, M., Ramonet, M., Wastine, B., Yver Kwok, C., Laurent, O., Belviso, S., Guemri, A., Philippon, C., Smith, J., and Conil, S.: Comparison of nitrous oxide (N_2O) analyzers for high-precision measurements of atmospheric mole fractions, Atmos. Meas. Tech., 9, 1221–1238, https://doi.org/10.5194/amt-9-1221-2016, 2016.

Lee, H. J., Jeong, S. E., Kim, P. J., Madsen, E. L., and Jeon, C. O.: High resolution depth distribution of Bacteria, Archaea, methanotrophs, and methanogens in the bulk and rhizosphere soils of a flooded rice paddy. Front. Microbiol., 6, 639, https://doi.org/10.3389/fmicb.2015.00639, 2015.

Lee, M., Nakane, K., Nakatsubo, T., Mo, W., and Koizumi, H.: Effects of rainfall events on soil CO_2 flux in a cool temperate deciduous broad-leaved forest, Ecol. Res., 17, 401–409. https://doi.org/10.1046/j.1440-1703.2002.00498.x, 2002.

Leitner S., Minixhofer P., Inselsbacher E., Keiblinger K.M., Zimmermann M., and Zechmeister-Boltenstern S.: Short-term soil mineral and organic nitrogen fluxes during moderate and severe drying–rewetting events, Appl. Soil Ecol., 114, 28–33, https://doi.org/10.1016/j.apsoil.2017.02.014, 2017.

Li, X., Ishikura, K., Wang, C., Yeluripati, J., and Hatano, R.: Hierarchical Bayesian models for soil CO_2 flux using soil texture: a case study in central Hokkaido, Japan, Soil Sci. Plant Nutr., 61, 116–132, https://doi.org/10.1080/00380768.2014.978728, 2015.

Liebig, M. A., Morgan, J. A., Reeder, J. D., Ellert, B. H., Gollany, H. T., and Schuman, G. E.: Greenhouse gas contributions and mitigation potential of agricultural practices in northwestern USA and Western Canada, Soil Tillage Res., 83, 25–52, https://doi.org/10.1016/j.still.2005.02.008, 2005.

Long, G. L. and Winefordner, J. D.: Limit of detection. A closer look at the IUPAC definition, Anal. Chem. 55, 712A– 724A, https://doi.org/10.1021/ac00258a001, 1983.

Lopez, M., Schmidt, M., Ramonet, M., Bonne, J.-L., Colomb, A., Kazan, V., Laj, P., and Pichon, J.-M.: Three years of semicontinuous greenhouse gas measurements at the Puy de Dôme station (central France), Atmos. Meas. Tech. 8, 3941–3958, https://doi.org/10.5194/amt-8-3941-2015, 2015.

Luo, G. J., Kiese, R., Wolf, B., and Butterbach-Bahl, K.: Effects of soil temperature and moisture on methane uptake and nitrous oxide emissions across three different ecosystem types, Biogeosciences, 10, 3205–3219, https://doi.org/10.5194/bg-10-3205-2013, 2013.

Mäki, M. J., Aalto, J., Hellén, H., Pihlatie, M., and Bäck, J.: Interannual and seasonal dynamics of volatile organic compound fluxes from the boreal forest floor, Front. Plant Sci., 10, 1–14, https://doi.org/10.3389/fpls.2019.00191, 2019.

Mancuso, S., Taiti, C., Bazihizina, N., Costa, C., Menesatti, P., Giagnoni, L., Arenella, M., Nannipieri, P., and Renella, G.: Soil volatile analysis by proton transfer reaction-time of flight mass spectrometry (PTR–TOF–MS), Appl. Soil Ecol., 86, 182–191, https://doi.org/10.1016/j.apsoil.2014.10.018, 2015.

Nakayama, N., Watanabe, S., and Tsunogai, S.: Nitrogen, oxygen and argon dissolved in the northern North Pacific in early summer, J. Oceanogr., 58, 775–785, https://doi.org/10.1023/A:1022810827059, 2002.

Nickerson, N.: Evaluating Gas Emission Measurements using Minimum Detectable Flux (MDF), Eosense Inc, Dartmouth, Canada, https://doi.org/10.13140/RG.2.1.4149.2089, 2016.

Nobre, A., Keller, M., Crill, P., and Harriss, R.: Short-term nitrous oxide profile dynamics and emissions response to water, nitrogen and carbon additions in two tropical soils, Biol. Fertil. Soils, 34, 363–373, https://doi.org/10.1007/s003740100396, 2001.

Minamikawa, K., Tokida, T., Sudo, S., Padre, A., and Yagi, K.: Guidelines for measuring CH_4 and N_2O emissions from rice paddies by a manually operated closed chamber method, National Institute for Agro-Environmental Sciences, Tsukuba, Japan, 2015.

Oertel, C., Matschullat, J., Zurbaa, K., Zimmermann, F., and Erasmi, S.: Greenhouse gas emissions from soils—a review, Geochem., 76, 327–352, https://doi.org/10.1016/j.chemer.2016.04.002, 2016.

Pärn J., Verhoeven, J. T., Butterbach-Bahl, K., Dise, N. B., Ullah, S., Aasa, A., Egorov, S., Espenberg, M., Järveoja, J., Jauhiainen, J., Kasak, K., Klemedtsson, L., Kull, A., Laggoun-Défarge, F., Lapshina, E. D., Lohila, A., Lõhmus, K., Maddison, M., Mitsch, W. J., Müller, C., Niinemets, Ü., Osborne, B., Pae, T., Salm, J. O., Sgouridis, F., Sohar, K., Soosaar, K., Storey, K., Teemusk, A., Tenywa, M. M., Tournebize, J., Truu, J., Veber, G., Villa, J. A., Zaw, S. S., and Mander, Ü.: Nitrogen-rich organic soils under warm well-drained conditions are global nitrous oxide emission hotspots, Nat. Commun., 9, 1–8, https://doi.org/10.1038/s41467-018-03540-1, 2018.

Peñuelas, J., Asensio, D., Tholl, D., Wenke, K., Rosenkranz, M., Piechulla, B., and Schnitzler, J. P.: Biogenic volatile emissions from the soil. Plant, Cell Environ., 37, 1866–1891, https://doi.org/10.1111/pce.12340, 2014.

Rowlings, D. W., Grace, P. R., Kiese, R., and Weier, K. L.: Environmental factors controlling temporal and spatial variability in the soil-atmosphere exchange of CO_2, CH_4 and N_2O from t, Glob. Change Biol., 18, 726–738, https://doi.org/10.1111/j.1365-2486.2011.02563.x, 2012.

Sainju, U. M., Stevens, W. B., Caesar-TonThat, T., and Liebig, M. A.: Soil greenhouse gas emissions affected by irrigation, tillage, crop rotation, and nitrogen fertilization. J. Environ. Qual., 41, 1774–1786, https://doi.org/10.2134/jeq2012.0176, 2012.

Schwenke, G. D. and Haigh, B. M.: The interaction of seasonal rainfall and nitrogen fertiliser rate on soil N_2O emission, total N loss and crop yield of dryland sorghum and sunflower grown on sub-tropical Vertosols, Soil Res., 54, 604–618, https://doi.org/10.1071/SR15286, 2016.

Shimma, S., Nagao, H., Aoki, J., Takahashi, K., Miki S., and Toyoda, M.: Miniaturized high-resolution time-of-flight mass spectrometer MULTUM-S II with an infinite flight path, Anal. Chem., 82, 8456–8463, https://doi.org/10.1021/ac1010348, 2010.

Smith, D. R. and Owens, P. R.: Impact of time to first rainfall event on greenhouse gas emissions following manure applications. Commun. Soil Sci. Plant Anal., 41, 1604–1614, https://doi.org/10.1080/00103624.2010.485240, 2010.

Szogs, S., Arneth, A., Anthoni, P., Doelman, J. C., Humpenöder, F., Popp, A., Pugh, T. A., and Stehfest, E.: Impact of LULCC on the emission of BVOCs during the 21st century, Atmos. Environ., 165, 73–87, https://doi.org/10.1016/j.atmosenv.2017.06.025, 2017.

Turcu, V. E., Jones, S. B., and Or, D.: Continuous soil carbon dioxide and oxygen measurements and estimation of gradient-based gaseous flux. Vadose Zone J., 4, 1161–1169, https://doi.org/10.2136/vzj2004.0164, 2005.

Toma, Y., Sari, N. N., Akamatsu, K., Oomori, S., Nagata, O., Nishimura, S., Purwanto, B. H., and Ueno, H.: Effects of green manure application and prolonging mid-season drainage on greenhouse gas emission from paddy fields in Ehime, Southwestern Japan. Agriculture, 9, 1–17, https://doi.org/10.3390/agriculture9020029, 2019.

Veres, P. R., Behrendt, T., Klapthor, A., Meixner, F. X., and Williams, J.: Volatile Organic Compound emissions from soil: using Proton-Transfer-Reaction Time-of-Flight Mass Spectrometry (PTR-TOF-MS) for the real time observation of microbial processes, Biogeosciences Discuss., 11, 12009–12038, https://doi.org/10.5194/bgd-11-12009-2014, 2014.

Yang, W. H. and Silver, W. L.: Application of the N_2/Ar technique to measuring soil-atmosphere N_2 fluxes: Measuring soil surface N_2 fluxes, Rapid Commun. Mass Spectrom., 26, 449–59, https://doi.org/10.1002/rcm.6124, 2012.

Yuan, B., Koss, A. R., Warneke, C., Coggon, M., Sekimoto, K., and de Gouw, J. A.: Proton-transfer-reaction mass spectrometry: Applications in atmospheric sciences, Chem. Rev., 117(21), 13187–13229, https://doi.org/10.1021/acs.chemrev.7b00325, 2017.

Table 1. Elapsed time between sample injection and corresponding adjustment of ion detector voltage in MULTUM to perform hybrid ion detection and signal processing (waveform averaging or ion counting) for specific target ions.

GC elapsed time (s)	Detector voltage (V)	Target gas	*m/z*	Data acquisition method
0	1400	-	-	-
48	2650	O^+	15.994	ion-counting
		CH_4^+	16.031	
73	2400	CO_2^+	44.001	waveform averaging
96	2650	N_2O^+	43.989	ion-counting
125	1400	-	-	-

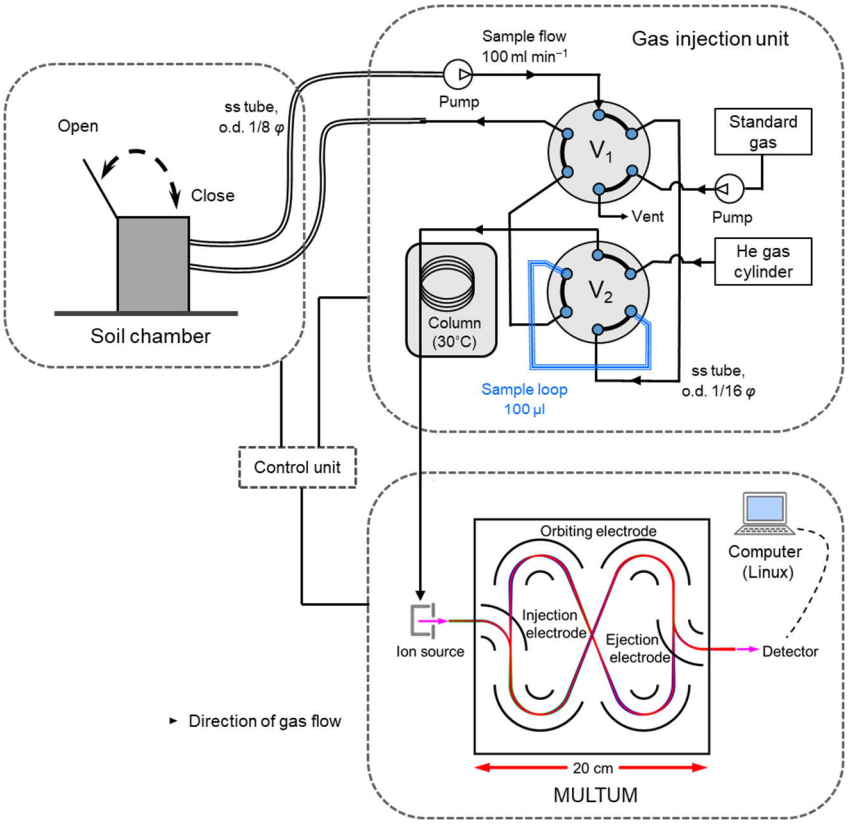

Figure 1. Schematic of developed mass spectrometric multiple soil-gas flux measurement system with a portable high-resolution multiturn time-of-flight mass spectrometer (MULTUM) coupled with an automated soil-gas flux chamber. The headspace gas in the chamber continuously circulates a sample loop in the gas injection unit through stainless-steel tubing. In each gas analysis, the headspace gas in the sample loop is injected into a capillary column for rough gas separation before analyzing each gas with MULTUM. (o.d., outer diameter; ss, stainless steel).

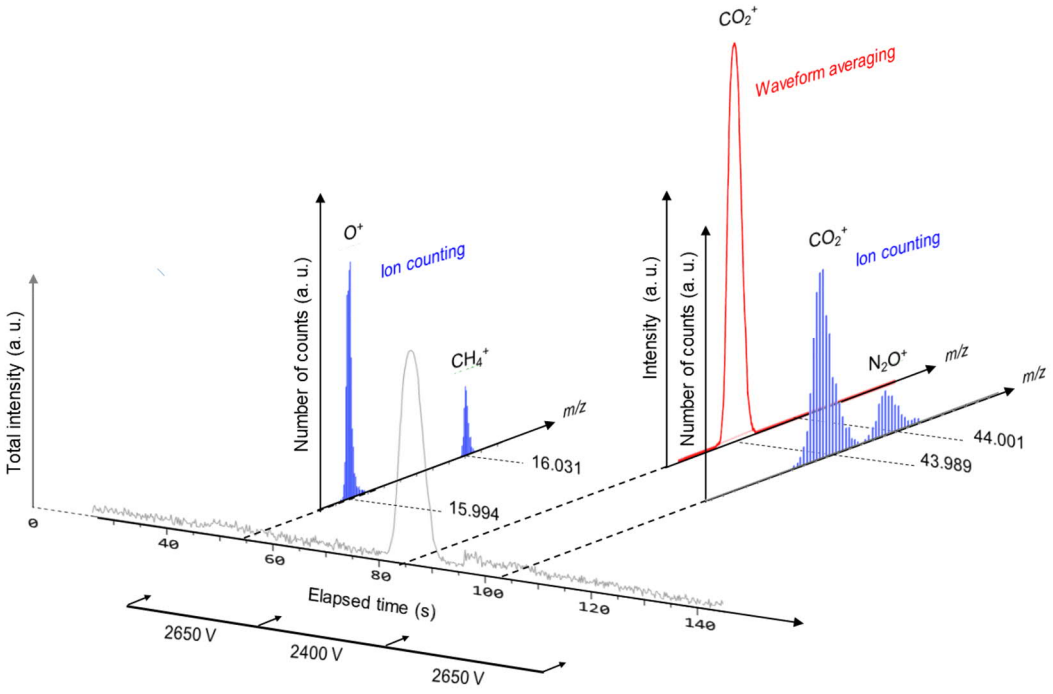

Figure 2. Schematic of two-dimensional gas/ion separation for O_2, CH_4, CO_2, and N_2O in chromatographic and *m/z* domains using a short column for rough separation and high-resolution mass spectrometry (MULTUM) for further complete separation. O_2, CH_4, and N_2O are detected as O^+, CH_4^+, and N_2O^+ with ion counting mode, whereas CO_2 is detected as CO_2^+ with waveform averaging mode. In the chromatographic domain, CO_2 and N_2O are not fully separated; however, in the *m/z* domain, residual contributions of CO_2^+ and N_2O^+ are fully separated by high mass resolving power of MULTUM.

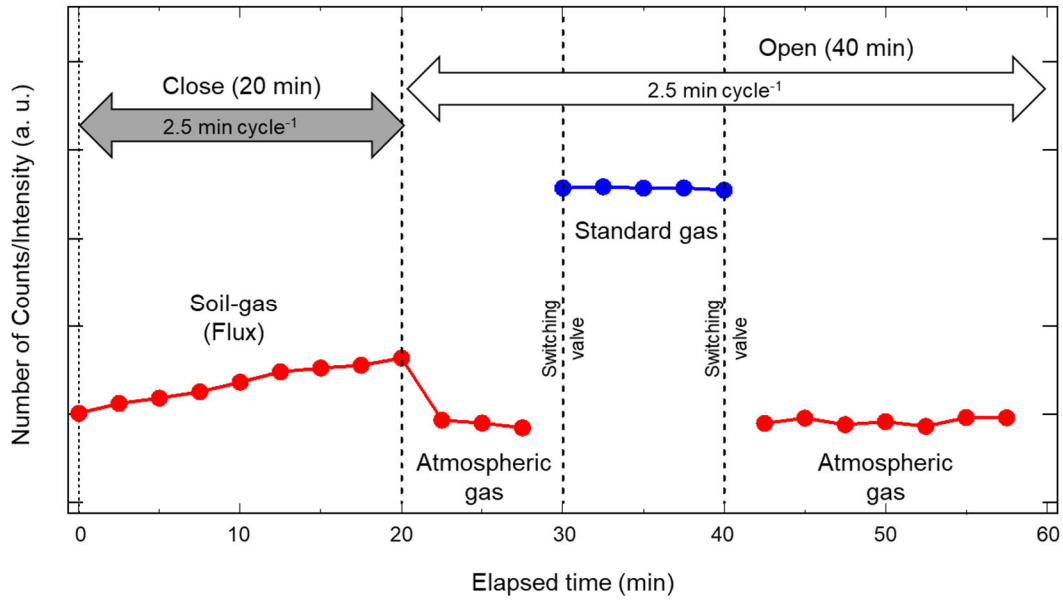

Figure 3. Example sequence of flux measurement conducted over 1 h and continued during field and laboratory flux observations. The flux chamber is closed for the first 20 min of flux measurement. During the remaining 40 min, the chamber is open and standard and atmospheric gas measurements are conducted for system stability verification and calibration.

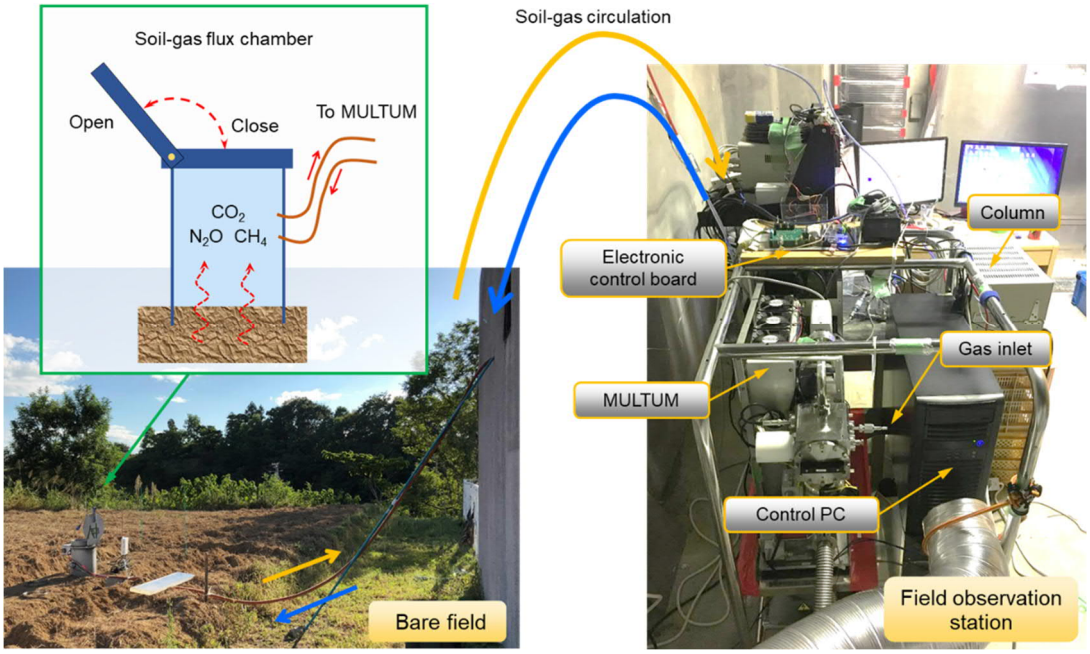

Figure 4. Instrument setup during a field flux campaign at the university farm of Ehime University (Matsuyama-shi, Ehime, Japan).

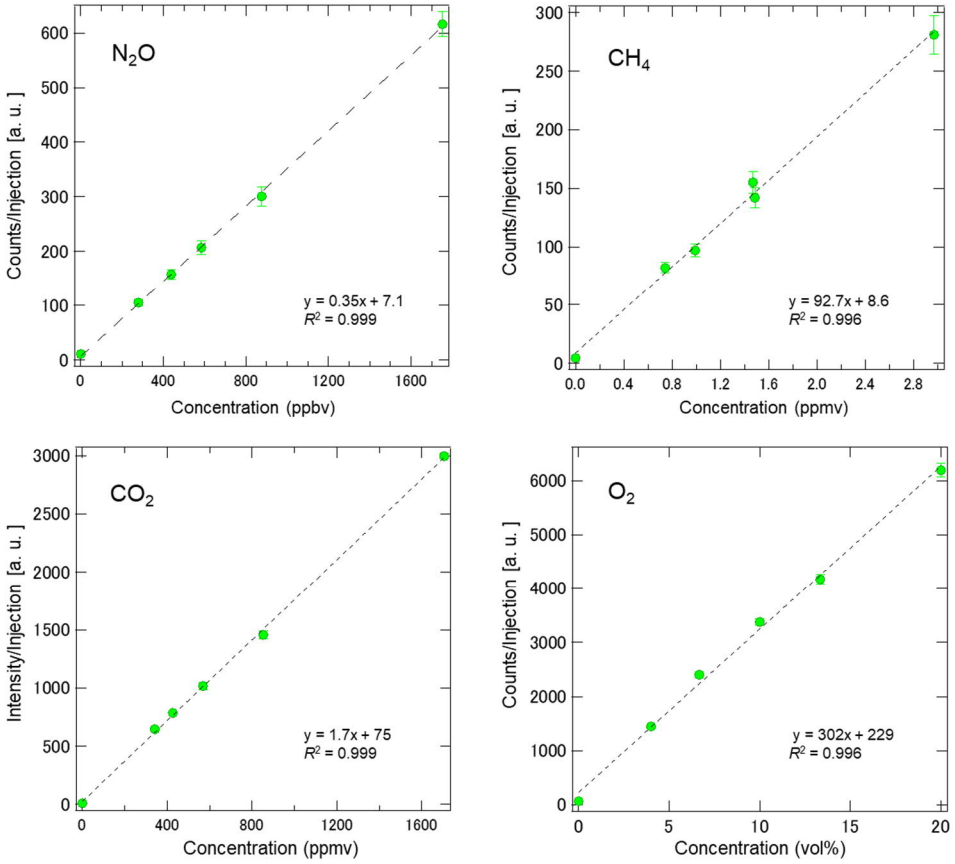

Figure 5. Calibration curves of MULTUM obtained by introducing standard gases of N_2O, CH_4, CO_2, and O_2 diluted by ultrapure N_2. The coefficients of determination (R^2) for each linear regressions were above 0.996 for all gases regardless huge concentration difference by six orders of magnitude. Each points were based on ten replicate injections.

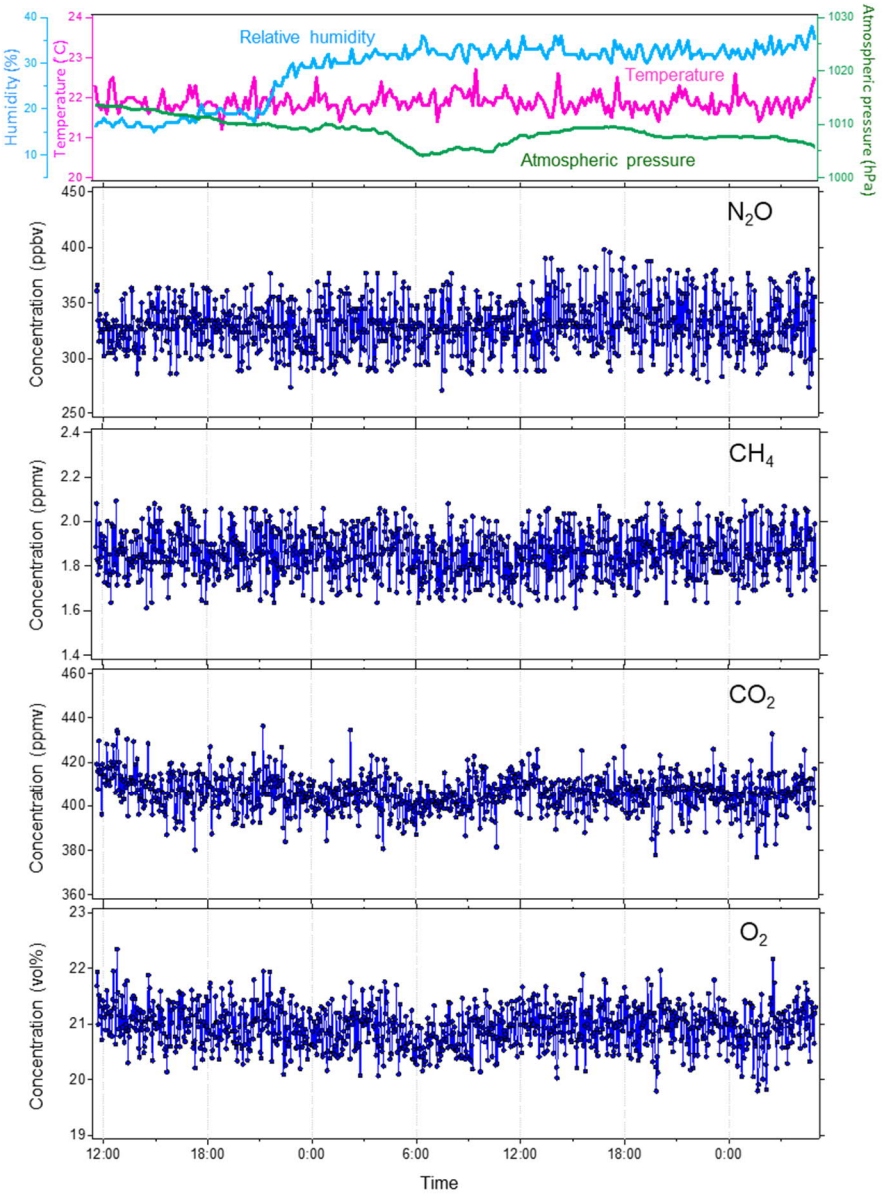

Figure 6. Continuous measurements of atmospheric N_2O, CH_4, CO_2, and O_2 in the laboratory with the soil chamber opened. Every 2.5 min, concentrations of the four gases were observed. The blue dots indicate individual data points. Top panel: the variations of atmospheric conditions during the laboratory measurement; atmospheric temperature (°C), pressure (hPa), and relative humidity (%).

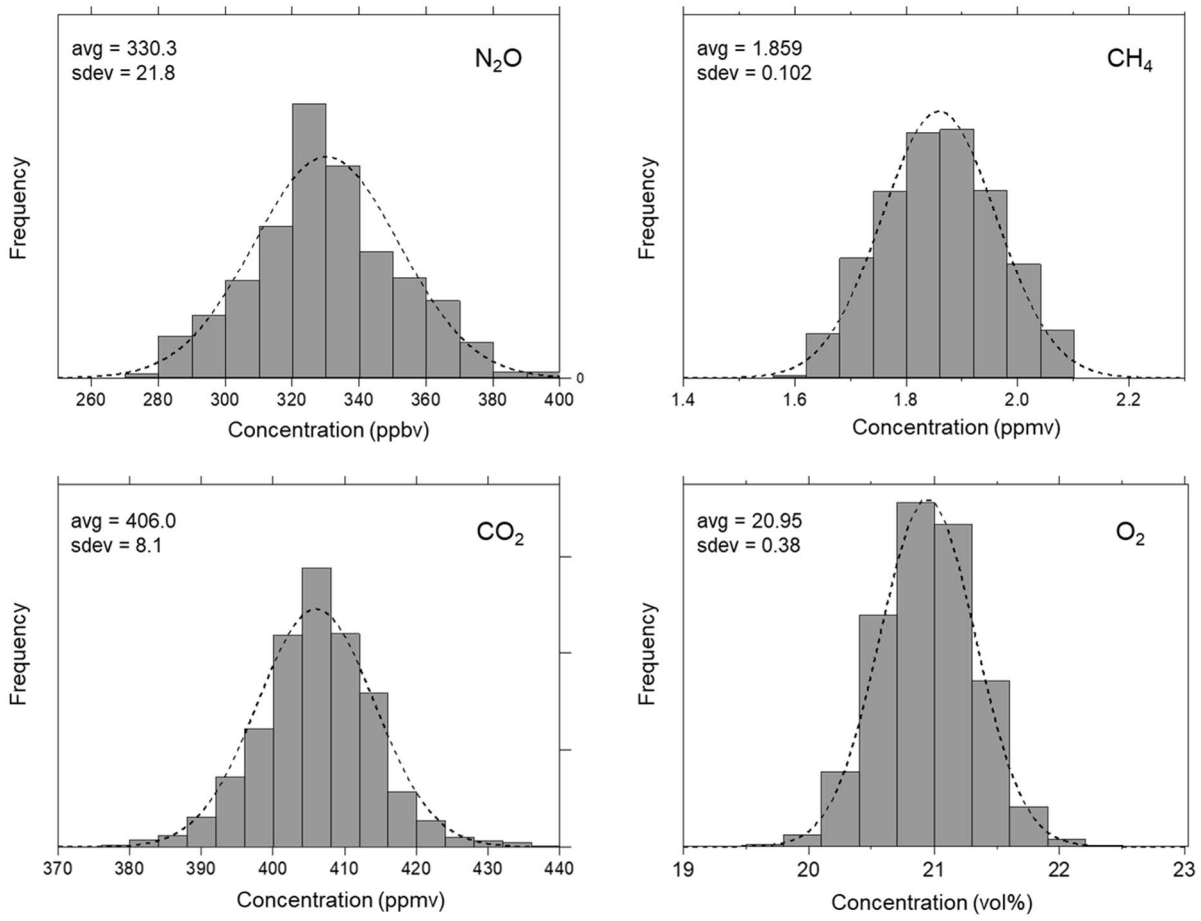

Figure 7. Frequency distributions of measured atmospheric concentrations of N_2O, CH_4, CO_2, and O_2 (994 measurements) during the laboratory measurement with the MULTUM-soil chamber system. For visual comparison, Gaussian distributions are plotted as dotted lines. Averages (avg) and standard deviations (sdev) shown in the panels were calculated from the atmospheric measurement for each gas species.

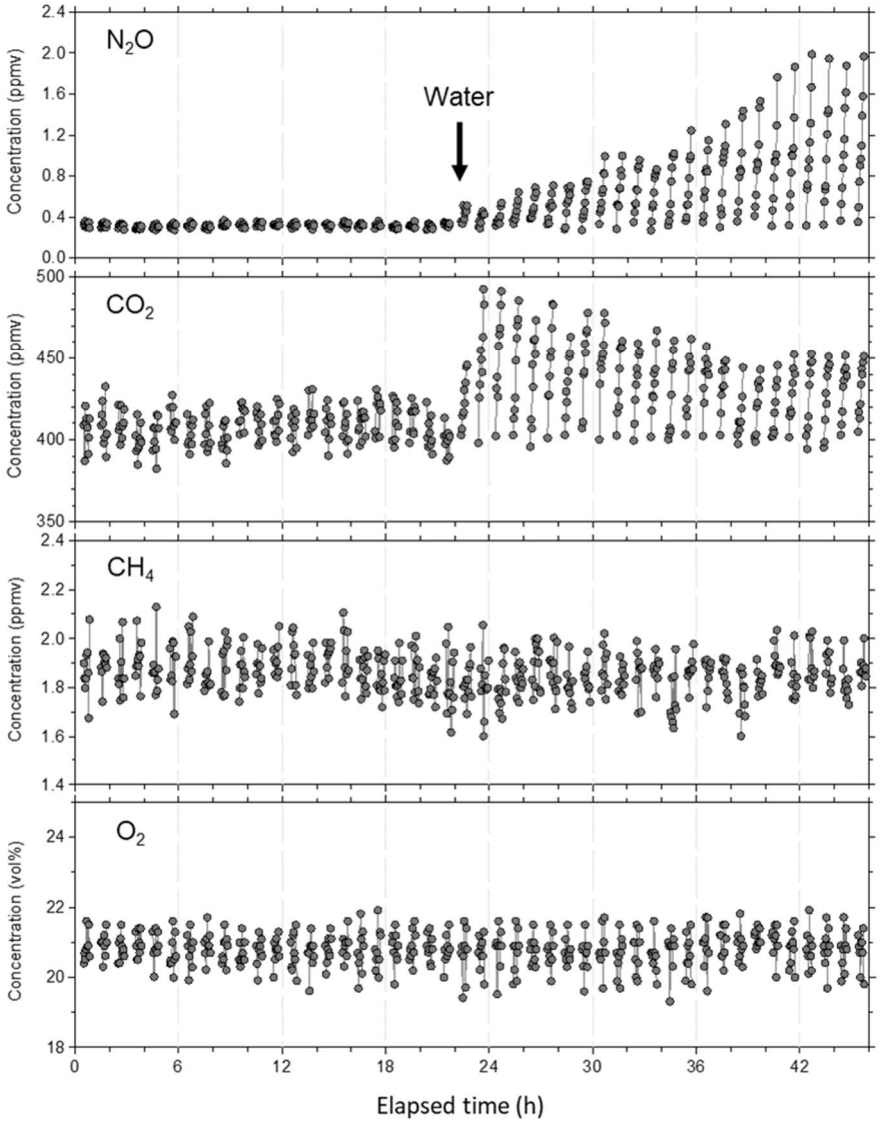

Figure 8. Example of continuous and simultaneous flux measurement of N_2O, CH_4, CO_2, and O_2 in the laboratory with a simulated plowed field. After 22 h, water (3 L) was sprayed on the soil surface. Immediately after the water addition, emission of N_2O and CO_2 began to change in different ways. For CH_4 and O_2, no flux beyond their minimum quantitative fluxes was observed throughout the flux measurement.

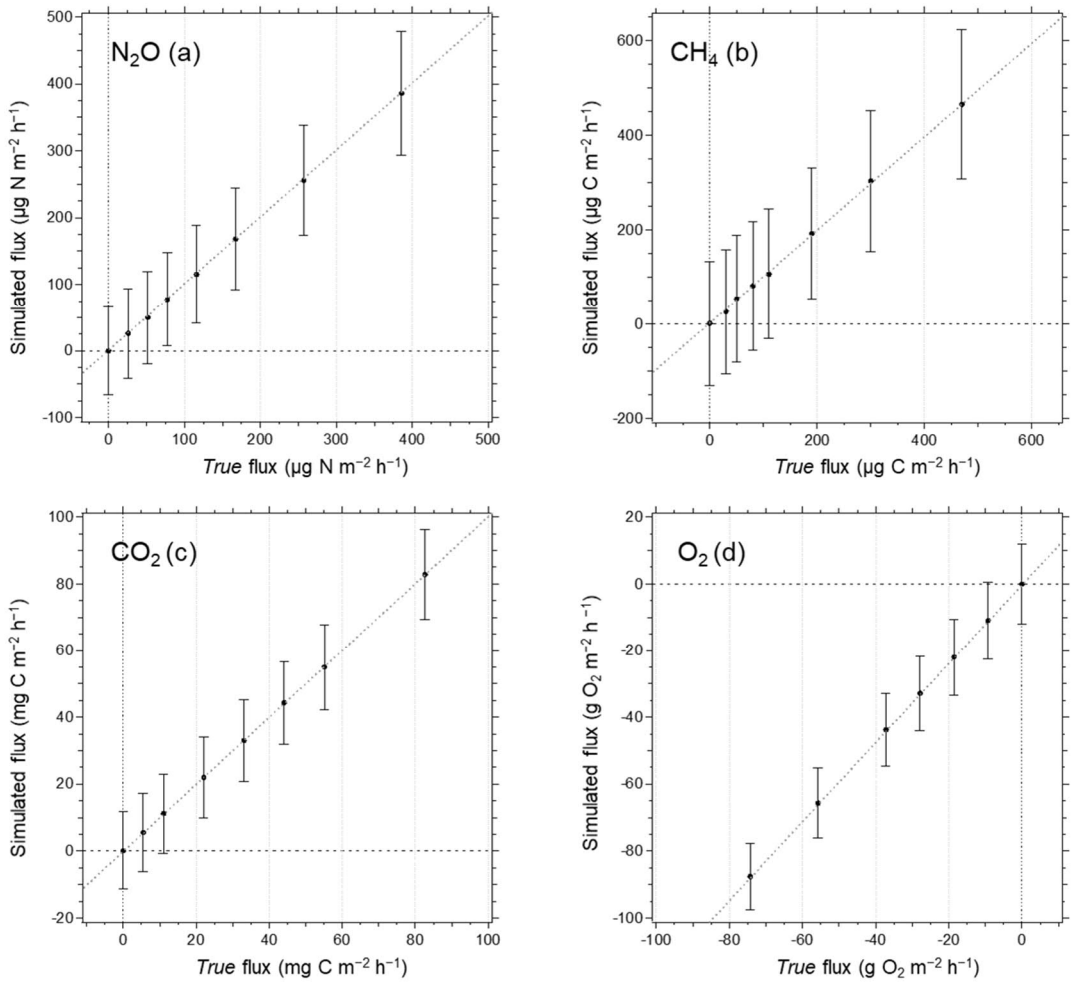

Figure 9. Relationship between *true* and simulated fluxes of (a) N_2O, (b) CH_4, (c) CO_2, and (d) O_2. In the simulated flux determination, random deviations of each gas concentration measurements were considered. The error bars in the figures represent two standard deviations of the fluxes derived from 10000 simulated flux measurements for each flux condition. The MQF is defined as a minimum quantitative flux when the *true* flux is equal to two standard deviations of simulated flux.

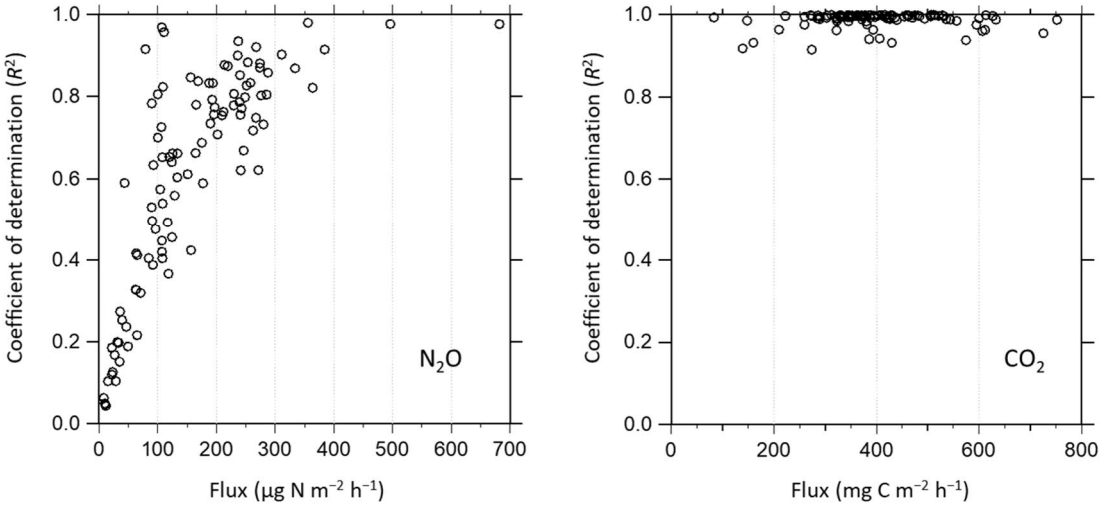

Figure 10. Relationship between determined fluxes during field observation and coefficient of determinations (R^2) in the linear regression to derive corresponding slopes (fluxes) from nine consecutive gas concentration observations per flux measurement.

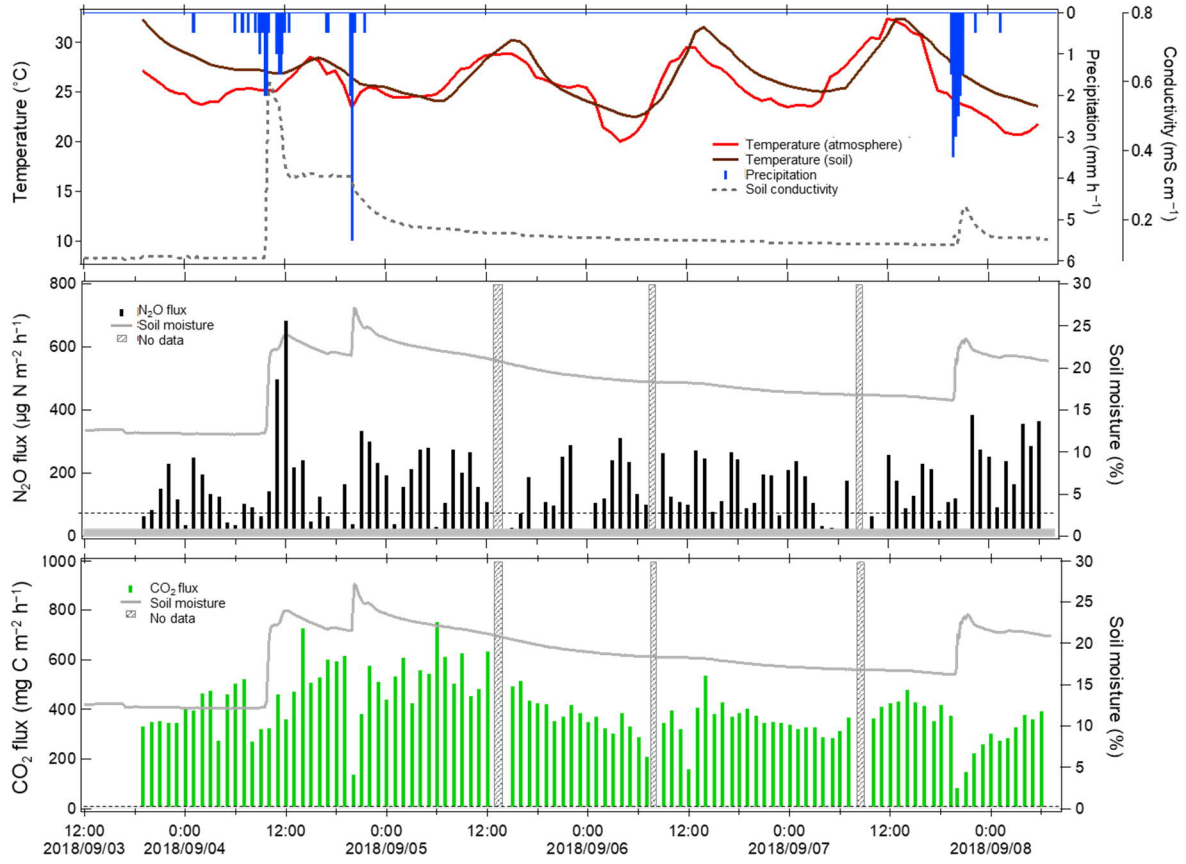

Figure 11. Temporal variations of observed N_2O and CO_2 fluxes at the university farm of Ehime University during field flux observation in September 2018. The dotted lines represent QMFs. Fluxes below the MDF are masked. The shaded areas represent no data due to measurement interruption by system issues, and so on.

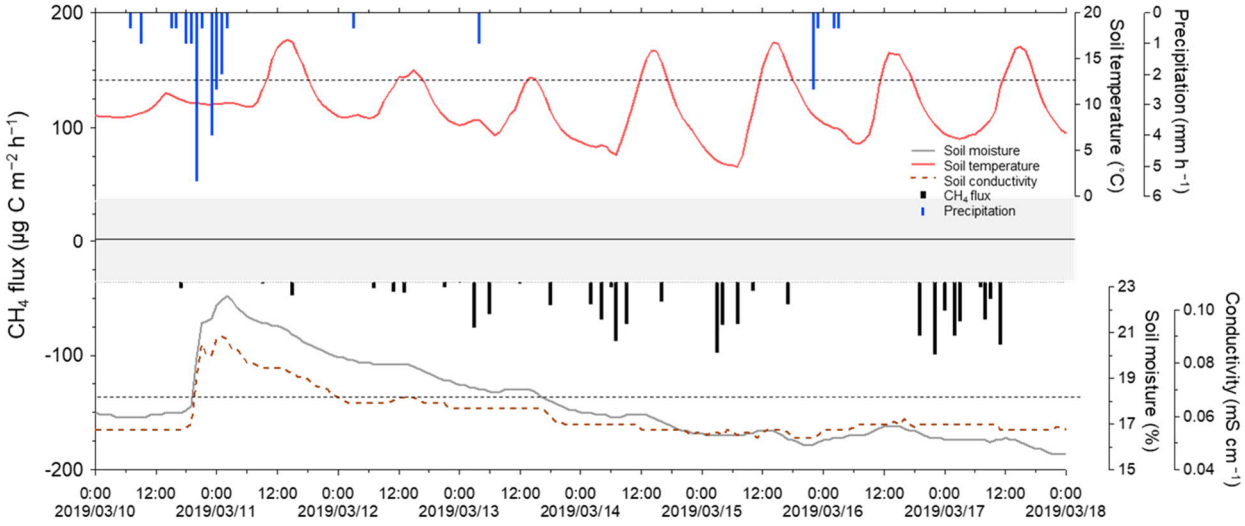

Figure 12. Temporal variations of observed CH_4 flux at the university farm of Ehime University during field flux observation in March 2019. Fluxes smaller than the MDF (35.4 μg C m^{-2} h^{-1}) are masked. Dotted grey lines represent the MQF (139 μg C m^{-2} h^{-1}).